Stress-structure coupling and nonlinear rheology of Lennard-Jones liquid

Tsuyoshi Yamaguchi

Citation: The Journal of Chemical Physics **148**, 234507 (2018); doi: 10.1063/1.5026536
View online: https://doi.org/10.1063/1.5026536
View Table of Contents: http://aip.scitation.org/toc/jcp/148/23
Published by the American Institute of Physics

Stress-structure coupling and nonlinear rheology of Lennard-Jones liquid

Tsuyoshi Yamaguchi[a)]
Graduate School of Engineering, Nagoya University, Furo-cho B2-3 (611), Chikusa, Nagoya, Aichi 464-8603, Japan

(Received 21 February 2018; accepted 5 June 2018; published online 21 June 2018)

The cross correlation between the two-body density and shear stress of Lennerd-Jones liquids is evaluated by means of equilibrium molecular dynamics (MD) simulation in order to clarify the microscopic structure that determines the shear viscosity. The slowest viscoelastic relaxation is coupled to the shift of the main peak of the static structure factor as is predicted by mode-coupling theory (MCT). The decay of the cross-correlation function in the reciprocal space is explained by the square of the intermediate scattering function, which is also in harmony with MCT. The distortion of the microscopic structure under simple shear is calculated by means of non-equilibrium MD simulation. The linear response relation also holds on the two-body density within the Newtonian regime of shear viscosity, while the structural distortion diminishes in the shear-thinning regime. The transition between the Newtonian and the shear-thinning regimes occurs at the shear rate where the magnitude of the structural distortion becomes as large as that of the equilibrium structure. The breakdown of the Cox-Merz rule is ascribed to the narrow width of the main peak of the static structure factor. *Published by AIP Publishing.* https://doi.org/10.1063/1.5026536

I. INTRODUCTION

Shear viscosity is a transport property that governs macroscopic flow of liquids.[1] Owing to its practical importance in physical chemistry, chemical engineering, mechanical engineering, and other fields, the data of the shear viscosity of liquids under various conditions have been accumulated so far. However, studies on microscopic mechanisms determining the shear viscosity are still in progress.

According to the Newtonian law of viscosity, the shear viscosity is defined as the linear response of shear stress to shear rate. The microscopic structure of normal liquids is isotropic in its equilibrium state. The application of shear rate induces the anisotropic distortion of the microscopic structure, which is the origin of the shear stress. Therefore, it is necessary to clarify what kind of liquid structure is coupled to shear flow to bring about shear stress in order to realize the microscopic mechanism of shear viscosity.

We recently proposed a theoretical framework to analyze the stress-structure coupling from molecular dynamics (MD) simulation[2] and applied it to liquid methanol[2] and water.[3] In the methanol case, we found the coupling between the shear stress and the prepeak structure, which was ascribed to the shear-induced reorientation of the linear hydrogen-bonding network. In the water case, the anisotropic distortion of the microscopic structure was similar to the variation of the isotropic structure against hydrostatic pressure. The tetrahedral hydrogen-bonding network was weakened along the compression axis, while it was strengthened along the expansion axis.

The systems to which we have applied our theoretical framework were limited to hydrogen-bonding liquids so far. In order to clarify what is specific to these hydrogen-bonding liquids and what holds for liquids in general, however, we need to apply the same framework to liquids without hydrogen-bonding for comparison. In this work, we show the stress-structure coupling of the Lennard-Jones (LJ) liquid evaluated in the same way. Since the LJ liquid has been regarded as a standard model of normal liquids, we believe that our present results can be a starting point to study the stress-structure coupling of liquids with various intermolecular interactions.

Our theoretical framework is to calculate the cross-correlation functions between the shear stress and two-body density by means of equilibrium MD simulation and to interpret them as the linear response of the two-body density to applied shear flow. The linear response theory holds between the shear rate and the shear stress by definition in the Newtonian regime of viscosity, where the applied shear rate is sufficiently small. Under the large shear rate, however, the shear stress no longer obeys the Newtonian law, and the nonlinear responses such as shear thinning are observed. The response of the microscopic structure is also nonlinear in the shear-thinning regime because the nonlinearly of the shear stress must originate in the nonlinear structural response.

Shear thinning is often observed in polymer melts and polymer solutions under mild conditions. The Cox-Merz rule is known to describe the shear thinning of polymeric systems.[4] It relates the nonlinear viscosity under the steady and strong shear rate, $\eta(\dot{\gamma})$, to the frequency-dependent linear complex viscosity under oscillatory shear flow, $\eta^*(\omega)$, at the corresponding values of the shear rate, $\dot{\gamma}$, and the angular frequency, ω.

[a)]E-mail: yamaguchi.tsuyoshi@material.nagoya-u.ac.jp

Although the viscosity of liquids composed of molecules of low molecular weights usually follows the Newtonian law under mild conditions, there are some situations in which shear thinning of such molecular liquids is important. The first one is lubrication oils in the elasto-hydrodynamic lubrication (EHL) regime. The pressure imposed on a lubricant at the contact point is quite high (~GPa) in the EHL regime, and the shear rate is also very large there. Shear thinning is observed even in low molecular-weight liquids under such an extreme condition, and the information on the shear thinning is essential to understand the lubrication in the EHL regime.

We measured both $\eta(\dot{\gamma})$ and $\eta^*(\omega)$ of three representative lubrication oils in our previous work.[5] We found that squalane follows the Cox-Merz rule fairly well, while the shear thinning of 2,4-dicyclohexyl-2-methylpentane (DCMP) and di(2-ethylhexyl)phthalate (DEHP) occurs at the shear rate several times smaller than the angular frequency of the viscoelastic relaxation. We tentatively ascribed the difference to that in their molecular shapes, that is, squalane is a long chain-like molecule, while the other two are not. However, it remains an unresolved question: what is the microscopic mechanism that relates the molecular shape and the Cox-Merz rule.

Supercooled liquid near glass transition is another system whose shear thinning attracts many researchers.[6–12] The relaxation time of a supercooled liquid shows rapid increase with decreasing temperature near the glass transition. The zero-shear viscosity also increases accordingly, and large shear thinning is reported there. With a belief that the shear thinning of supercooled liquids reflects essential dynamics related to the glass transition, it has been investigated intensively for decades. The shear thinning of supercooled liquids has mainly been studied computationally or theoretically on model systems composed of spherical particles. Large deviation from the Cox-Merz rule has been reported, that is, the shear thinning occurs more than ten times faster than the prediction of the Cox-Merz rule. Many mechanisms have been proposed so far to explain the shear thinning and the breakdown of the Cox-Merz rule of the supercooled liquid.[6–12]

This work is performed for the following two purposes. The first one is to understand the linear stress-structure coupling of the LJ liquid as a standard model of normal liquids. The second one is to evaluate the distortion of the microscopic structure of the LJ liquid by means of non-equilibrium MD simulation and to compare it with the linear response prediction estimated from equilibrium MD simulation. The origin of the shear thinning and the breakdown of the Cox-Merz rule is discussed based on the nonlinearity of the structural distortion.

II. THEORY

Suppose that simple shear flow is applied to liquids as

$$\mathbf{v}(\mathbf{r}) = \dot{\gamma} y \hat{\mathbf{x}}, \tag{1}$$

where $\mathbf{v}(\mathbf{r})$ stands for the velocity field at the position $\mathbf{r}$, and $\hat{\boldsymbol{x}}$ denotes the unit vector of the x-direction. The position-independent constant $\dot{\gamma}$ is called the "shear rate." The Newtonian law of viscosity states that the xy-component of the shear part of the pressure tensor is proportional to the shear rate as

$$P_{xy}^{(\mathrm{s})}(\dot{\gamma}) = -\eta_s \dot{\gamma}. \tag{2}$$

The proportionality constant, η_s, is called "shear viscosity." Here, $\mathbf{P}^{(\mathrm{s})}$ is the traceless and symmetric part of the pressure tensor, $\mathbf{P}$, as

$$\mathbf{P}^{(s)} \equiv \frac{1}{2}\left(\mathbf{P} + \mathbf{P}^t\right) - \frac{1}{3}[\mathrm{Tr}\,\mathbf{P}]\mathbf{I}. \tag{3}$$

The linear response relation, Eq. (2), breaks down when the applied shear rate is sufficiently large. The shear-rate dependent shear viscosity, $\eta(\dot{\gamma})$, is then defined as

$$\eta(\dot{\gamma}) \equiv -\frac{P_{xy}^{(s)}(\dot{\gamma})}{\dot{\gamma}}. \tag{4}$$

The decrease in $\eta(\dot{\gamma})$ with increasing $\dot{\gamma}$ is called "shear thinning."

The linear Newtonian law of viscosity, Eq. (2), can also be extended to the frequency-dependent one. When the weak oscillatory shear rate, $\dot{\gamma}(t) = \dot{\gamma}_\omega \exp(-i\omega t)$, is applied to the liquid, the linear response of $\mathbf{P}^{(\mathrm{s})}$ is also oscillatory as

$$P_{xy}^{(\mathrm{s})}(\dot{\gamma}_\omega; t) = -\eta^*(\omega)\dot{\gamma}_\omega e^{-i\omega t}, \tag{5}$$

which defines the frequency-dependent complex shear viscosity, $\eta^*(\omega)$.

The linear response theory relates the linear response of a system to a weak external field with the spontaneous fluctuation of the system without the external field. When it is applied to the pressure tensor under shear, it gives the well-known Kubo-Green formula of viscosity as[13]

$$\eta^*(\omega) = \int_0^\infty dt\, e^{-i\omega t} G(t), \tag{6}$$

$$G(t) \equiv \frac{V}{k_B T}\left\langle P_{xy}^{(s)}(t=0) P_{xy}^{(s)}(t)\right\rangle_{eq}. \tag{7}$$

Here, k_B, T, and V stand for the Boltzmann constant, the absolute temperature, and the volume of the system, respectively. The suffix "eq" in Eq. (7) means the statistical average under the equilibrium ensemble.

The structure of simple liquids is often described in terms of the two-body density defined as

$$\rho^{(2)}(\mathbf{q}) \equiv \tilde{\rho}^*(\mathbf{q})\tilde{\rho}(\mathbf{q}), \tag{8}$$

where $\tilde{\rho}(\mathbf{q})$ stands for the density field in the reciprocal space. Its equilibrium average gives the static structure factor, $S(q)$, as

$$S(|\mathbf{q}|) = \frac{1}{\rho V}\left\langle \rho^{(2)}(\mathbf{q})\right\rangle_{eq}. \tag{9}$$

The number density of molecules is denoted as ρ here. Although the structure factor is isotropic under the equilibrium condition, it is anisotropically distorted under the shear flow given by Eq. (1). The spherical harmonics expansion is applied to the anisotropic structure factor as

$$S^{ne}(\mathbf{q};\dot\gamma) \equiv \frac{1}{\rho V}\left\langle \rho^{(2)}(\mathbf{q})\right\rangle_{\dot\gamma} = S_{iso}(|\mathbf{q}|;\dot\gamma) - \frac{q_x q_y}{|\mathbf{q}|^2} S_{xy}(|\mathbf{q}|;\dot\gamma) + O\left(\dot\gamma^2\right). \quad (10)$$

The suffix $\dot\gamma$ attached to the angular bracket indicates the non-equilibrium average under the shear rate $\dot\gamma$. In the zero-shear limit, only the first isotropic term survives and it reduces to the static structure factor, $S(q)$. Because the shear flow possesses the xy-symmetry, it couples linearly solely with the second term, $S_{xy}(q;\dot\gamma)$. The remaining terms of the spherical harmonic expansion are nonlinear to $\dot\gamma$. The minus sign is introduced to the second term so that it describes the variation of the structure factor along the complex axis of the shear deformation.

The linear response theory relates $S_{xy}(|\mathbf{q}|;\dot\gamma)$ to an equilibrium correlation function as

$$\lim_{\dot\gamma\to 0}\frac{\rho S_{xy}(|\mathbf{q}|;\dot\gamma)}{\dot\gamma} = \int_0^\infty dt\, \rho_\eta^{(2)}(q,t), \quad (11)$$

$$\rho_\eta^{(2)}(q,t) \equiv \frac{|\mathbf{q}|^2}{k_B T q_x q_y}\left\langle P_{xy}^{(s)}(t=0)\delta\rho^{(2)}(\mathbf{q},t)\right\rangle_{eq}, \quad (12)$$

$$\delta\rho^{(2)}(\mathbf{q},t) \equiv \rho^{(2)}(\mathbf{q},t) - \left\langle \rho^{(2)}(\mathbf{q},t)\right\rangle_{eq}. \quad (13)$$

The function $\gamma\rho_\eta^{(2)}(q,t)$ describes the linear response of the structure factor to the delta-function like shear rate, $\dot\gamma(t) = \gamma\delta(t)$, which in turn is equivalent to the instantaneous shear deformation γ.

The initial value of $\rho_\eta^{(2)}(q,t)$ is related to the derivative of the static structure factor as

$$\rho_\eta^{(2)}(q,t=0) = -\rho q\frac{d}{dq}S(q). \quad (14)$$

The compression axis shrinks in a uniform way by the factor of $(1-\gamma/2)$ after the instantaneous shear deformation of γ. The structure factor thus expands in the uniform way as

$$S(q) \to S((1-\gamma/2)q) \cong S(q) - \frac{\gamma q}{2}\frac{d}{dq}S(q), \quad (15)$$

which explains Eq. (14).

The real-space counterpart of the two-body density is defined as

$$\rho^{(2r)}(\mathbf{r}) \equiv \frac{1}{V}\int d\mathbf{R}\,\rho(\mathbf{R}+\mathbf{r})\rho(\mathbf{R}). \quad (16)$$

Its equilibrium average defines the radial distribution function, $g(r)$, as

$$\left\langle \rho^{(2r)}(\mathbf{r})\right\rangle_{eq} \equiv \rho\delta(\mathbf{r}) + \rho^2 g(|\mathbf{r}|). \quad (17)$$

The real- and reciprocal-space representations of the two-body density, $\rho^{(2r)}(\mathbf{r})$ and $\rho^{(2)}(\mathbf{q})$, respectively, are related with each other through the Fourier transformation as

$$\int d^3\mathbf{r}\, e^{i\mathbf{q}\cdot\mathbf{r}}\rho^{(2r)}(\mathbf{r}) = \rho^{(2)}(\mathbf{q}). \quad (18)$$

The radial distribution function is also extended to the non-equilibrium one under the shear flow as

$$g^{ne}(\mathbf{r};\dot\gamma) \equiv \frac{1}{\rho^2}\left[\left\langle \rho^{(2r)}(\boldsymbol{r};\dot\gamma)\right\rangle_{\dot\gamma} - \rho\delta(\boldsymbol{r})\right] = g_{iso}(|\mathbf{r}|;\dot\gamma) - \frac{r_x r_y}{|\mathbf{r}|^2}g_{xy}(|\mathbf{r}|;\dot\gamma) + O\left(\dot\gamma^2\right). \quad (19)$$

The first term reduces to $g(r)$ in the zero-shear limit, while the second term is proportional to $\dot\gamma$. The linear response of $g_{xy}(r;\dot\gamma)$ is given by the equilibrium time correlation function as

$$\lim_{\dot\gamma\to 0}\frac{g_{xy}(|\mathbf{r}|;\dot\gamma)}{\dot\gamma} = \int_0^\infty dt\, g_\eta(r,t), \quad (20)$$

$$g_\eta(r,t) \equiv \frac{|\mathbf{r}|^2}{k_B T r_x r_y}\left\langle P_{xy}^{(s)}(t=0)\delta\rho^{(2r)}(\mathbf{r},t)\right\rangle_{eq}, \quad (21)$$

$$\delta\rho^{(2r)}(\mathbf{r},t) \equiv \rho^{(2)}(\mathbf{r},t) - \left\langle \rho^{(2)}(\mathbf{r},t)\right\rangle_{eq}. \quad (22)$$

The initial value of $g_\eta(r,t)$ is related to the radial distribution function as

$$g_\eta(r,t=0) = r\frac{d}{dr}g(r), \quad (23)$$

which can also be understood in terms of uniform compression as is the case of Eq. (15).

The pressure tensor is divided as the sum of the kinetic and the interaction parts, and the latter usually dominates in dense liquids. When the intermolecular interaction is described by the pairwise-additive potential function, $u(r)$, the instantaneous value of the interaction part of $P^{(s)}{}_{xy}$, denoted as $P^{(I,s)}{}_{xy}$, is given by

$$P_{xy}^{(I,s)} = -\frac{1}{2}\int d^3\mathbf{r}\frac{r_x r_y}{|\mathbf{r}|}\cdot\frac{du(r)}{dr}\cdot\rho^{(2r)}(\mathbf{r}). \quad (24)$$

Combining Eqs. (19) and (24), the statistical average of $P^{(I,s)}{}_{xy}$ under shear is described as follows:

$$\left\langle P_{xy}^{(I,s)}\right\rangle_{\dot\gamma} = \frac{2\pi\rho^2}{15}\int_0^\infty dr r^3\frac{du(r)}{dr}g_{xy}(r;\dot\gamma). \quad (25)$$

Therefore, $g_{xy}(r;\dot\gamma)$ describes the structural deformation that determines the shear rheology of liquids.

The theoretical formulation above is exact in principle. The functions $\rho_\eta^{(2)}(q,t)$ and $g_\eta(r,t)$ can be evaluated by equilibrium MD simulation according to their definitions, Eqs. (12) and (23), respectively. The non-equilibrium pair correlation functions, $S^{ne}(\mathbf{q};\dot\gamma)$ and $g^{ne}(\mathbf{r};\dot\gamma)$ are obtained by non-equilibrium MD simulation, and their spherical-harmonics expansion gives $S_{iso}(q;\dot\gamma)$, $S_{xy}(q;\dot\gamma)$, $g_{iso}(r;\dot\gamma)$, and $g_{xy}(r;\dot\gamma)$.

In addition to the computational approach using MD simulation, analytical approaches using mode-coupling theory (MCT) have been employed for linear and nonlinear rheological properties of liquids. MCT was originally developed for the dynamics of liquids in the equilibrium state and intensively applied to study the slow dynamics of supercooled liquids.[14] Since the equilibrium MCT treats the fluctuation of density modes in the equilibrium state, its target in rheology is limited to linear viscoelasticity. In 2002, Fuchs and Cates extended MCT to describe the liquid dynamics under shear,[6,7] and MCT treatments of liquid dynamics under shear have been developed further by several researchers.[8,15,16] The

MCT under shear was applied to the nonlinear rheology of supercooled liquids and succeeded in reproducing strong shear thinning.[6–8,16]

MCT possesses some advantages over MD simulation owing to its analytical character. First, it can access extremely slow dynamics that MD simulation cannot handle due to the limitation of the capability of current computers. It can also treat asymptotic behaviors of various correlation functions near the non-ergodic transition. On the other hand, it suffers from various approximations which are inevitable in analytical theories. Among them, the most important one is the factorization approximation, which is common to both equilibrium and non-equilibrium MCT. Two-body density is a natural descriptor of the liquid structure as was already discussed in this section. In particular, its real-space representation is closely related to the shear pressure tensor as is described by Eq. (24). We treat the two-body density, both the real- and reciprocal-space ones, in an exact and explicit way using MD simulation. In MCT, on the other hand, the dynamic variable of consideration is usually the one-body density in the reciprocal space, $\tilde{\rho}(\mathbf{q})$, and the factorization approximation is employed for the dynamics of the fluctuation of the two-body density, assuming the Gaussian statistics of $\tilde{\rho}(\mathbf{q})$.

In this work, the factorization approximation in MCT is examined by applying it to $\rho_\eta^{(2)}(q,t)$. The factorization-version of $\rho_\eta^{(2)}(q,t)$ is given by the square of the intermediate scattering function, $F(q,t)$, as[2]

$$\rho_\eta^{(2)}(q,t) \cong -\rho^2 q \frac{dc(q)}{dq}[F(q,t)]^2, \tag{26}$$

$$F(|\mathbf{q}|,t) \equiv \frac{1}{\rho V}\langle \tilde{\rho}^*(\mathbf{q},t=0)\tilde{\rho}(\mathbf{q},t)\rangle_{eq}, \tag{27}$$

where the direct correlation function, $c(q)$, is defined as[13]

$$c(q) \equiv \frac{1}{\rho}\left[1 - \frac{1}{S(q)}\right]. \tag{28}$$

In addition to the factorization approximation above, the non-equilibrium MCT usually accompanies an approximation of the fluctuation-dissipation theorem, which relates the response of a variable to an external field to the thermal fluctuation of the variable without the field, as is exemplified by Eq. (7) for the shear stress. Although the fluctuation-dissipation theorem holds in equilibrium systems, it may not hold in non-equilibrium systems such as liquids under shear.[8,11]

III. MD SIMULATION

The equilibrium and non-equilibrium MD simulation runs of the LJ liquid were performed. All the physical quantities are hereafter given in the reduced unit, where the well-depth (ε) and the diameter (σ) parameters of the LJ potential, the mass of the molecule (m), and the Boltzmann constant are unity. In particular, the unit of the shear viscosity is given by $\sqrt{\varepsilon m}/\sigma^2$. The temperature and the number density of the system are 0.75 and 0.85, respectively, which is a liquid state near the triple point.

The system is composed of 1000 LJ particles, which are filled within an initially cubic cell with periodic boundary conditions. The simple shear was applied in the seven non-equilibrium runs, and the magnitudes of the shear rates were $\dot{\gamma}$ = 0.01, 0.02, 0.05, 0.1, 0.2, 0.5, and 1, respectively. All the simulation runs were performed under the NVT ensemble, and the temperature of the system was controlled with a Nosé-Hoover thermostat.[17] The equation of motion was integrated with the leap-frog algorithm with the time step of 0.001. For each shear rate, the system was waited to reach the equilibrium or the steady-state for 10^6 steps, and the trajectory of the subsequent 10^7 steps was analyzed. All the simulation runs were performed using the GROMACS 5.1.2 package.[18]

IV. RESULTS AND DISCUSSION

A. Equilibrium simulation

Figure 1 shows $G(t)$ and its running integral calculated from the equilibrium MD simulation. The time correlation function $G(t)$ is composed of a fast binary collision part within $t < 0.2$ and the slow tail. The running integral converges within $t < 2$, yielding the value of the shear viscosity of 3.2 in the LJ reduced unit. The shear viscosity is consistent with the value we determined in a previous work under the same condition.[19] The slow tail explains about half of the steady-state shear viscosity.

The real-space version of the cross-correlation function between the two-body density and the shear pressure tensor is shown in Fig. 2. Figure 2(a) shows the equilibrium radial distribution function for reference. The cross-correlation functions $g_\eta(r,t)$ at various times are exhibited in Fig. 2(b) as the function of r. The initial profile is given by the derivative of $g(r)$ as is predicted by Eq. (23). The profile then decays with time accompanied by a small change in its pattern. Closely looking at the dynamics within the first peak of $g(r)$, the decay at $t < 0.1$ is faster than that at larger r, and the shift of the differential profile to larger r is observed within $t < 0.1$. It is in harmony with the idea that the fast decay of $G(t)$ at $t < 0.1$ is assigned to the binary collision. The time-integrated profile is shown in Fig. 2(c), which is equivalent to the distortion of the two-body density under weak shear flow. The shape of the integrated profile is similar to $g_\eta(r,t)$ after the binary collision. The differential-shaped profile shown in Fig. 2(c) indicates that $g(r)$ is compressed along the compression axis

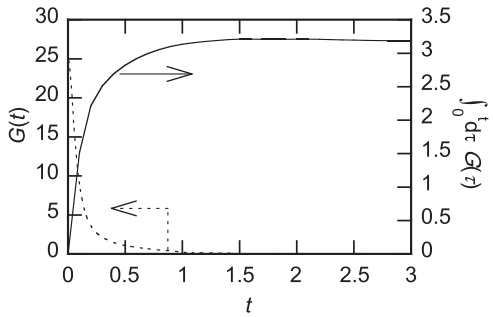

FIG. 1. The time correlation function $G(t)$ (dotted) and its running integral (solid) are plotted as the function of time.

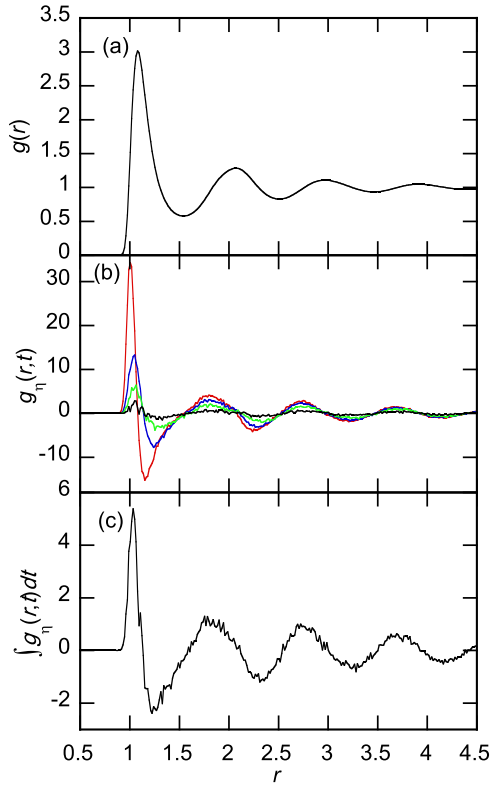

FIG. 2. The real-space version of the equilibrium structure and the cross-correlation functions between the two-body density and the shear stress are plotted. The radial distribution function, $g(r)$, is shown in panel (a). The cross correlation functions $g_\eta(r,t)$, defined by Eq. (21), at $t = 0$ (red), 0.1 (blue), 0.2 (green), and 0.5 (black) are shown in panel (b). The integral of $g_\eta(r,t)$ over $0 < t < 2$ is shown in panel (c).

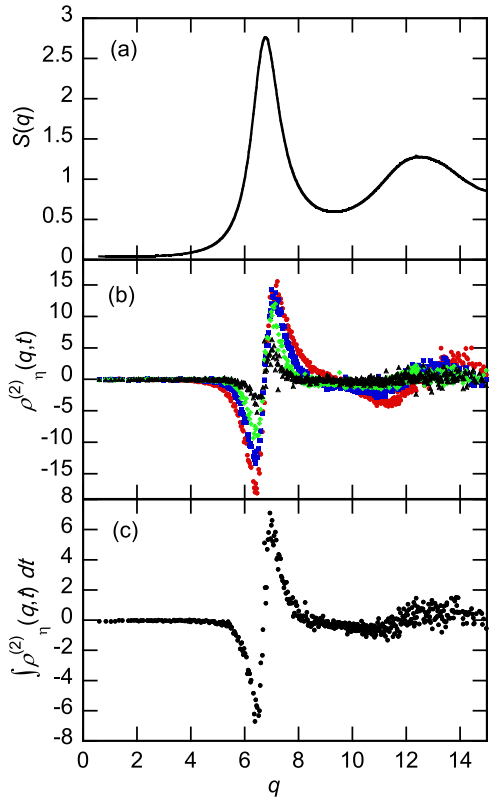

FIG. 3. The reciprocal-space version of the equilibrium structure and the cross-correlation functions between the two-body density and the shear stress are plotted. The static structure factor, $S(q)$, is shown in panel (a). The cross correlation functions $\rho^{(2)}{}_\eta(q,t)$, defined by Eq. (12), at $t = 0$ (red), 0.1 (blue), 0.2 (green), and 0.5 (black) are shown in panel (b). The integral of $\rho^{(2)}{}_\eta(q,t)$ over $0 < t < 2$ is shown in panel (c).

under shear, which is in harmony with non-equilibrium MD simulation on supercooled liquids performed by Ingebringtsen and Tanaka.[20]

The reciprocal space version of the cross-correlation function, $\rho^{(2)}_\eta(q,t)$, is exhibited in Fig. 3. The static structure factor is shown in Fig. 3(a) for reference, which is characterized by a strong peak at $q = 6.8$. This peak, which is hereafter called the "main peak" reflects the long-ranged oscillation of the radial distribution function in Fig. 2(a). The correlation functions $\rho^{(2)}_\eta(q,t)$ at various times are plotted as the function of q in Fig. 3(b). The initial profile is given by the derivative of $S(q)$ as is predicted by Eq. (14). The decay of the high-q structure around $q \sim 12$ is fast, while the dynamics at the main peak is slow. As a result, the integrated profile shown in Fig. 3(c) is dominated by the differential-shaped structure at the main peak. The fast high-q dynamics in the reciprocal space in Fig. 3(b) reflects the binary dynamics at the first peak of $g(r)$ in the real space in Fig. 2(b). The slow relaxation of the profile at the main peak in Fig. 3(b) corresponds to that of the long-ranged oscillation in Fig. 2(b). The differential-shaped profile at the main peak of $S(q)$ means the anisotropic shift of the main peak according to Eq. (15). Considering its dominance in the time-integrated profile, Fig. 3(c), it can be said that the shear viscosity of the LJ liquid is governed by the anisotropic shift of the main peak of the structure factor. The importance of the structural dynamics on the shear viscosity was already suggested based on equilibrium MCT,[21] and it is also consistent with experiments.[22]

In our previous studies, we reported the stress-structure coupling of two representative hydrogen-bonding liquids, water[3] and methanol.[2] The coupling in these hydrogen-bonding liquids is quite different from that of the LJ liquid in many aspects. The most important difference is the fast structural rearrangement of the hydrogen-bonding liquids within the binary-collision time regime. The cross-correlation functions $\rho^{(2)}_\eta(q,t)$ of water and methanol after the binary collision, $t \sim 100$ fs, appear quite different from the corresponding initial profiles. The positive profile appears at the prepeak in methanol, and the anisotropic destruction-formation of the network structure is observed in water. In the LJ liquid, the change in the profile near the main peak is rather small in the binary-collision time regime, although the fast relaxation is observed in the high-q region.

Figure 4 shows the time profiles of $\rho^{(2)}_\eta(q,t)$ at their two strong peaks, the negative peak at $q = 6.4$ and the positive one at $q = 7.1$. The decay rates of these two peaks are close to each other, and this decay rate describes the relaxation rates of the anisotropic shift of the main peak of the structure factor. Compared with the viscoelastic relaxation, $G(t)$, the relaxation of the two peaks explains the slow tail part of $G(t)$.

The decay of these two peaks is also compared with the prediction of the factorization approximation employed in MCT, Eq. (26). The intermediate scattering function in the rhs of Eq. (26), $F(q,t)$, was determined from the same MD simulation separately. The decay of the cross correlation function

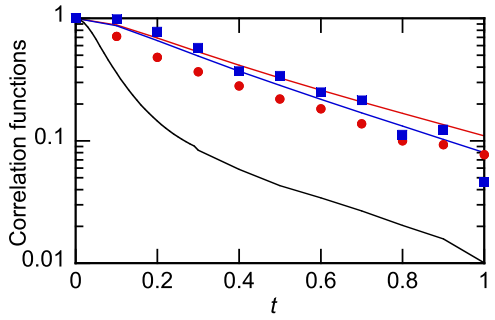

FIG. 4. The time profiles of $\rho^{(2)}{}_{\eta}(q,t)$ given by Eq. (12) at the negative peak, $q = 6.4$, and the positive peak, $q = 7.1$, are plotted with the red circles and the blue squares, respectively. The squares of the intermediate scattering function at the corresponding values of q are shown with the solid curves of the corresponding colors. The stress autocorrelation function, $G(t)$, is plotted with the black solid curve. All the correlation functions are normalized to their respective initial values.

follows that of the square of the intermediate scattering function well, as is demonstrated in Fig. 4, indicating the success of the factorization approximation.

The physical picture of the microscopic origin of the shear relaxation of the LJ liquid obtained from the cross-correlation analysis of the equilibrium MD simulation is summarized as below. The application of the instantaneous shear distortion induces the anisotropic shift of the main peak of the structure factor. The peak shifts to higher-q along the compression axis, while it shifts to lower-q along the expansion axis. The anisotropic shift of the main peak gives the transient shear stress, which relaxes at the relaxation rate of the peak shift. The dynamics of the peak shift is then described by the square of the intermediate scattering function, in accordance with the MCT picture. The structural dynamics around the main peak of the structure factor governs the shear viscosity of the LJ liquid in this way.

B. Non-equilibrium simulation

The results of non-equilibrium MD simulation under shear flow are compared with the prediction of the linear response theory in this subsection. First, the shear-rate dependent shear viscosity, $\eta(\dot\gamma)$, is shown as the function of the shear rate, $\dot\gamma$, in Fig. 5. The complex shear viscosity calculated from $G(t)$ in Fig. 1, $\eta^*(\omega)$, is plotted together for comparison. The low-frequency limiting value of $\eta^*(\omega)$ gives the steady-state shear viscosity.

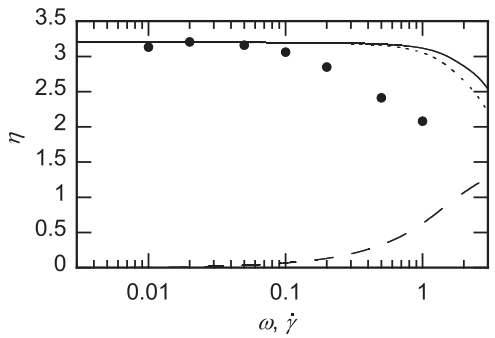

FIG. 5. The shear-rate dependent non-equilibrium viscosity, $\eta(\dot\gamma)$ defined by Eq. (4), is plotted with the filled circles as the function of the shear rate, while the real part (dotted), the imaginary part (dashed), and the amplitude (solid) of the equilibrium frequency-dependent complex shear viscosity, $\eta^*(\omega)$ given by Eq. (6), are shown as the function of the angular frequency.

The non-equilibrium shear viscosity follows the Newtonian law at $\dot\gamma < 0.1$, while the shear thinning is clearly observed at $\dot\gamma > 0.2$. The transition shear rate between the Newtonian and the shear thinning regimes is thus determined to be 0.1–0.2. The presence of the shear thinning in the LJ liquid has been reported since the beginning of the non-equilibrium MD simulation.[23] On the other hand, the deviation of the amplitude of the frequency-dependent complex shear viscosity, $|\eta^*(\omega)|$, from the low-frequency limiting value occurs at the angular frequency $\omega \sim 1$. Therefore, the nonlinear shear viscosity of the LJ liquid does not follow the Cox-Merz rule, and the shear thinning occurs at the shear rate several times lower than that predicted by the Cox-Merz rule.

The violation of the Cox-Merz rule has been reported by many researchers on model liquids composed of spherical particles such as the LJ one.[11,12] Experimentally, we found that the shear thinning of two lubrication oils, DCMP and DEHP, occurs at the shear rate several times lower than the Cox-Merz prediction.[5] Our present result in Fig. 5 is thus in harmony with the preceding results in literatures.

The non-equilibrium two-body correlation functions in the real space, $g^{ne}(\mathbf{r};\dot\gamma)$, at various values of the shear rate are plotted as the function of r in Fig. 6. The isotropic part, $g_{iso}(r;\dot\gamma)$, is shown in Fig. 6(a) and compared with the

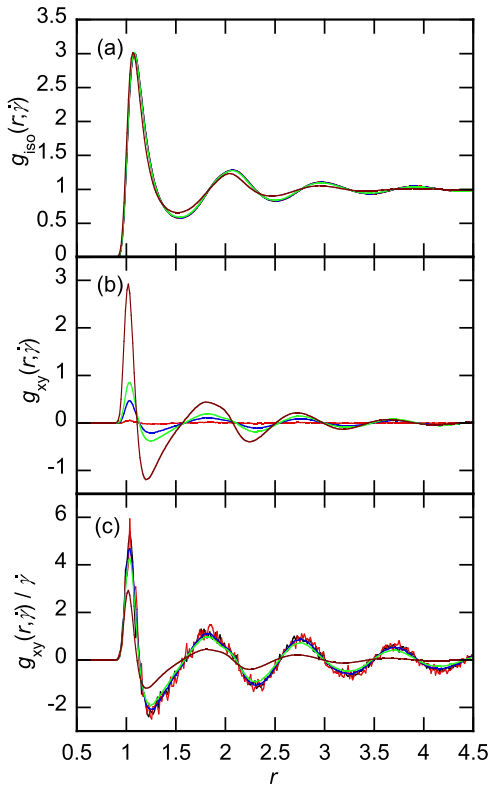

FIG. 6. The isotropic part, $g_{iso}(r;\dot\gamma)$ and the anisotropic part, $g_{xy}(r;\dot\gamma)$, defined by Eq. (19), of the distribution functions under shear flow are plotted in panels (a) and (b), while the normalization of the latter to the shear rate, $g_{xy}(r;\dot\gamma)/\dot\gamma$, is shown in panel (c). The values of the shear rate, $\dot\gamma$, are 0.01 (red), 0.1 (blue), 0.2 (green), and 1 (brown), respectively. The corresponding equilibrium functions are also shown in panels (a) and (c) with black curves.

corresponding equilibrium function. The isotropic part scarcely depends on the shear rate within the Newtonian regime of the shear viscosity, which is consistent with the theoretical prediction that the leading term of the change in $g_{iso}(r;\dot\gamma)$ with $\dot\gamma$ is $O\left(\dot\gamma^2\right)$. The deviation from the equilibrium function is apparent at the onset of the shear thinning, $\dot\gamma = 0.2$. Comparing the function at $\dot\gamma = 1$ with the equilibrium one, it should be noticed that the most significant change in the isotropic part is the smearing out of the long-range oscillation. Similar behavior was already reported by Ingebringtsen and Tanaka on supercooled liquids.[20] Since the long-range oscillation of $g(r)$ corresponds to the narrow main peak of the static structure factor, the smearing out of the oscillation means the diminishing and the broadening of the main peak of the structure factor. Miyazaki and co-workers calculated the structure factor of a model supercooled liquid under shear and reported the change in the main peak of the structure factor as described above.[8]

Compared with the large change in $g_{iso}(r;\dot\gamma)$ at large r, its variation within the first peak of $g(r)$ is rather marginal. The height of the first peak is almost independent of the shear rate, while the peak position slightly shifts to the smaller r. Furukawa argued that the effective radius of the molecules decreases under shear, which reduces the effective density, leading to the decrease in the shear viscosity through the decrease in the structural relaxation time.[12] The shift of the first peak in Fig. 6(a) can actually be interpreted as the decrease in the effective radius. On the other hand, the local density within the first solvation shell does not decrease with the shear rate. However, if we employ the strength of the main peak of the structure factor as a measure of the effective packing fraction, the smearing out of the long-range oscillation of $g_{iso}(r;\dot\gamma)$ is regarded as the decrease in the effective density.

The xy-component of the non-equilibrium two-body correlation function, $g_{xy}(r;\dot\gamma)$, is exhibited in Fig. 6(b). The shape of the profile is similar to the prediction of the linear response, Fig. 2(c), and its amplitude increases with increasing the shear rate. Compared with $g(r)$, we would like to point out that the amplitude of the long-range oscillation of $g_{xy}(r;\dot\gamma)$ is comparable to that of $g(r)$ at the onset of the shear thinning. In short, the nonlinear rheology appears when the structural deformation is as large as the original equilibrium structure.

Figure 6(c) normalizes $g_{xy}(r;\dot\gamma)$ with respect to $\dot\gamma$ in order to test the linear response prediction, Eq. (20), quantitatively. The linear response prediction holds well on the two-body density in the Newtonian regime of the shear viscosity as expected, and the amplitude of the normalized response decreases with the shear rate in the shear-thinning regime. The nonlinearity in the first peak region of $g(r)$ is a little weaker than that of the long-range oscillation.

The characteristics of the nonlinear distortion of the two-body density under shear flow are summarized as follows: The shear thinning occurs when the amplitude of the long-range oscillation of $g_{xy}(r;\dot\gamma)$ is comparable to that of $g(r)$. In the shear-thinning regime, the oscillation of $g_{xy}(r;\dot\gamma)$ becomes smaller than the linear response prediction, and the smearing out of the long-range oscillation of the isotropic structure, $g_{iso}(r;\dot\gamma)$, is also observed.

Based on the results described above, we would like to propose a mechanism that can explain the breakdown of the Cox-Merz rule in the case of the LJ liquid. The position of the main peak of the static structure factor is denoted as q_0. In the linear response regime, Eq. (15) states that the peak shifts to $(1 + \gamma/2)q_0$ along the compression axis after the application of the instantaneous shear flow, $\dot\gamma(t) = \gamma\delta(t)$. According to Fig. 4, the shifted peak relaxes to the equilibrium one with the time constant τ_η, which is equal to the relaxation time of the slow tail part of $G(t)$. Therefore, the steady-state shift of the main peak of the structure factor is $\dot\gamma\tau_\eta q_0/2$ under the constant shear rate of $\dot\gamma$.

Figure 6(b) suggests that the shear thinning occurs when the distortion of the long-range oscillation of $g_{xy}(r;\dot\gamma)$, which corresponds to the anisotropic peak shift of the structure factor, is as large as the equilibrium structure. It is mathematically described as

$$\dot\gamma\tau_\eta q_0/2 \cong w_q, \tag{29}$$

that is, the peak shift is close to the half-width of the main peak of the static structure factor, w_q. Equation (29) is transformed as

$$\dot\gamma\tau_\eta \cong \frac{2w_q}{q_0}. \tag{30}$$

Due to the narrow width of the main peak of the structure factor, w_q is much smaller than q_0. In the present case, the peak position is $q_0 = 6.8$, while the full-width at the half maximum (fwhm) is $2w_q = 1.4$. Therefore, the shear thinning can occur at the shear rate several times smaller than $1/\tau_\eta$.

The nonlinearity of the shear stress begins when the microscopic structure under shear deviates from the equilibrium one, and the criteria of the distortion of the microscopic structure is the main peak of the static structure factor because the structural dynamics around the main peak governs the slow mode of the viscoelastic relaxation.

There can be two ways how the structural distortion leads to the shear thinning. The first one is the anharmonicity of the free-energy profile associated with the distortion of the structure factor. In the Ornstein-Zernike integral-equation theory of liquids formulated by Morita and Hiroike,[24] the free energy of the system is described as the functional of the pair correlation functions, and the equilibrium correlation functions are determined to minimize the free-energy functional. The distortion of the structure factor from the equilibrium one thus accompanies the free energy cost. The free-energy profile along the distortion is anharmonic when the deviation from the equilibrium structure is large, which can be an origin of the nonlinear response of the structure factor to the shear flow. The second one is that the distortion of the structure affects the structural relaxation time. The mechanism of the shear thinning of supercooled liquids proposed by Furukawa belongs to the second one.[12] The decrease in the structural relaxation time with increasing the shear rate was obtained by calculations on supercooled liquids using non-equilibrium MCT.[6–8] Provided that the dynamics of supercooled liquids near the glass transition is very sensitive to the structural change, small change in the structure factor may affect the dynamics of supercooled liquid, leading to the strong shear thinning.

Provided that many studies on the shear thinning of supercooled liquids focus on the decrease in the structural relaxation time under shear, it would be meaningful to exhibit time correlation functions of our normal LJ liquid under shear. We define here the time correlation function of the shear pressure tensor under shear as follows:

$$G^{ne}_{\alpha\mu}(t;\dot\gamma) \equiv \left(1-\frac{1}{4}\delta_{\alpha\mu}\right)\frac{V}{k_BT}\left\langle\left\{P^{(s)}_{\alpha\mu}(t=0)-\left\langle P^{(s)}_{\alpha\mu}\right\rangle_{\dot\gamma}\right\}\times\left\{P^{(s)}_{\alpha\mu}(t)-\left\langle P^{(s)}_{\alpha\mu}\right\rangle_{\dot\gamma}\right\}\right\rangle_{\dot\gamma}, \tag{31}$$

where α, $\mu \in \{x, y, z\}$ are suffices to indicate the three-dimensional components of the tensors. The prefactor $(1 - \delta_{\alpha\mu}/4)$ is introduced so that all the components of $G^{ne}_{\alpha\mu}(t;\dot\gamma)$ agree with one another in the equilibrium limit. The similar correlation functions were already calculated by Mizuno and Yamamoto on supercooled liquids in order to examine the fluctuation-dissipation theorem.[11]

Figure 7 shows the running integral of $G^{ne}_{xy}(t;\dot\gamma)$ at various values of shear rate. The variation of $G^{ne}_{xy}(t;\dot\gamma)$ with $\dot\gamma$ is rather small at $\dot\gamma \le 0.2$, and a large increase in the integrated value is observed in the strongly sheared system, $\dot\gamma = 1$. Closely looking at the time profile, the time scale of the relaxation of $G^{ne}_{xy}(t;\dot\gamma)$ decreases with increasing the shear rate as is expected. However, the decrease in the relaxation time does not lead to the decrease in the integrated value. In spite of the shear thinning at $\dot\gamma \ge 0.2$, the integrated value of $G^{ne}_{xy}(t;\dot\gamma)$ rapidly increases there. Therefore, under the sheared condition, the response of the shear stress to the variation of the shear rate is not described by the fluctuation of the shear stress. The increase in the integrated value is explained by the increase in the fast binary-collision component, which in turn is ascribed to the penetration of the first peak of $g_{iso}(r;\dot\gamma)$ into the repulsive core as is exhibited in Fig. 6(a). The rapid increase in the integrated value between $\dot\gamma = 0.2$ and 1 is thus ascribed to the large change in $g_{iso}(r;\dot\gamma)$. The breakdown of the fluctuation-dissipation theorem was already reported on supercooled liquids by Mizuno and Yamamoto,[11] and our results in Fig. 7 are in harmony with theirs.

The anisotropy of the dynamics of shear stress at $\dot\gamma = 1$ is examined in Fig. 8. The presence of the small but finite anisotropy is recognized, as was reported by Mizuno and Yamamoto on supercooled liquids.[11] The integrated values of the xx and yy components are larger than the zz one. Provided that the shear flow is applied in the xy-plane, it is quite natural that its effect is the smallest on the zz component.

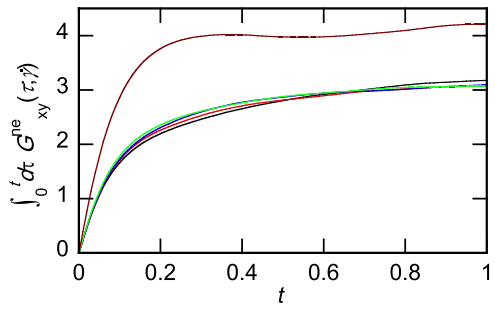

FIG. 7. The running integrals of the xy-components of the time correlation functions of the shear stress under shear flow, $G^{ne}_{xy}(t;\dot\gamma)$, defined by Eq. (31), are plotted as the function of time. The values of the shear rates are 0 (black; equilibrium), 0.01 (red), 0.1 (blue), 0.2 (green), and 1 (brown), respectively.

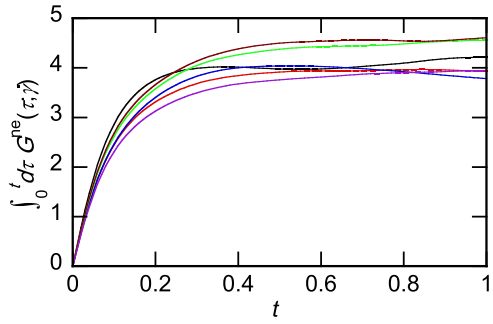

FIG. 8. The running integrals of the various components of the time correlation functions of the shear stress under shear flow, $G^{ne}_{\alpha\mu}(t;\dot\gamma)$, defined by Eq. (31), at $\dot\gamma = 1$ are plotted as the function of time. The different components are shown with different colors as xy (black), yz (red), zx (blue), xx (green), yy (brown), and zz (purple).

V. CONCLUSION

The microscopic origin of the viscoelastic relaxation and shear thinning of the LJ liquid was analyzed by means of equilibrium and non-equilibrium MD simulations. The cross-correlation analysis showed that the anisotropic shift of the main peak of the structure factor governs the shear viscosity through the slow mode of the viscoelastic relaxation. The relaxation of the cross-correlation function in the main peak region was described well by the square of the intermediate scattering function as is predicted by MCT. The structural rearrangement within the binary-collision time regime was small and limited to the high-q region in contrast to the large rearrangement in cases of water and methanol.

The shear thinning was observed in non-equilibrium MD simulation at the shear rate several times smaller than that predicted by the Cox-Merz rule. The linear response approximation for the distortion of the two-body density held well within the Newtonian regime of the shear viscosity. The shear thinning began at the shear rate when the long-range oscillation of the anisotropic part of the pair distribution function was comparable to that of the radial distribution function. In the shear-thinning regime, the isotropic part of the two-body density showed the smearing out of the long-range oscillation, which corresponded to the weakening and the broadening of the main peak of the structure factor. The anisotropic part of the structural distortion became smaller than the linear response prediction in the shear-thinning regime, and the weakening of the distortion was larger at the long-range oscillation than at the first peak of the radial distribution function.

A mechanism of the breakdown of the Cox-Merz rule was proposed based on the observation above. The nonlinearity of the shear stress was considered to occur when the anisotropic shift of the main peak of the structure factor is comparable to the width of the main peak because the slow dynamics of the shear stress is governed by the structural dynamics around

the main peak. Due to the narrow width of the main peak, small peak shifts induced by the shear flow can easily exceed the peak width, which explains the onset of the shear thinning at the shear rate smaller than the prediction of the Cox-Merz rule.

The mechanism above applies to various liquids whose viscoelastic relaxation is dominated by the anisotropic shift of the main peak of the static structure factor. We believe that the breakdown of the Cox-Merz rule on two lubrication oils, DCMP and DEHP,[5] belongs to this category. However, there are many dynamic modes that can be coupled to the slowest mode of the viscoelastic relaxation. For example, the translation-orientation coupling explains the slowest viscoelastic relaxation of liquids composed of rod-like molecules such as *n*-alkanes.[25] The viscoelastic relaxation of 1-alcohols is ascribed to the structural dynamics at the prepeak.[25,26] The dynamics of the tetrahedral network structure is responsible for the slow viscoelastic mode of liquid water.[3] The appearance of the nonlinear rheology will depend on the dynamic mode that governs the slowest viscoelastic relaxation mode, and we consider that the validity or the breakdown of the Cox-Merz rule on various liquids should be discussed from the view of the microscopic origin of shear viscosity.

ACKNOWLEDGMENTS

This work was supported by the Japan Society for the Promotion of Science (JSPS), KAKENHI Grant No. 16K05514.

[1] R. B. Bird, W. E. Stewart, and E. N. Lightfoot, *Transport Phenomena*, 2nd ed. (John Wiley & Sons, 2007).
[2] T. Yamaguchi and A. Faraone, J. Chem. Phys. **146**, 244506 (2017).
[3] T. Yamaguchi, J. Phys. Chem. B **122**, 1255 (2018).
[4] W. P. Cox and E. H. Merz, J. Polym. Sci. **28**, 619 (1958).
[5] S. Bair, T. Yamaguchi, L. Brouwer, H. Schwarze, P. Vergne, and G. Poll, Tribol. Int. **79**, 126 (2014).
[6] M. Fuchs and M. E. Cates, Phys. Rev. Lett. **89**, 248304 (2002).
[7] M. Fuchs and M. E. Cates, Faraday Discuss. **123**, 267 (2003).
[8] K. Miyazaki, D. R. Reichman, and R. Yamamoto, Phys. Rev. E **70**, 011501 (2004).
[9] A. Furukawa, K. Kim, S. Saito, and H. Tanaka, Phys. Rev. Lett. **102**, 016001 (2009).
[10] T. Voigtmann, Curr. Opin. Colloid Interface Sci. **19**, 549 (2014).
[11] H. Mizuno and R. Yamamoto, Eur. Phys. J. E **35**, 29 (2012).
[12] A. Furukawa, Phys. Rev. E **95**, 012613 (2017).
[13] J. P. Hansen and I. R. McDonald, *Theory of Simple Liquids*, 2nd ed. (Academic Press, 1986).
[14] W. Götze, *Complex Dynamics of Glass-Forming Liquids: A Mode-Coupling Theory* (Oxford University, 2009).
[15] S.-H. Chong and B. Kim, Phys. Rev. E **79**, 021203 (2009).
[16] K. Suzuki and H. Hayakawa, Phys. Rev. E **87**, 012304 (2013).
[17] M. P. Allen and D. J. Tildesley, *Computer Simulation of Liquids* (Oxford University Press, 1987).
[18] M. J. Abraham, T. Murtola, R. Schulz, S. Pall, J. C. Smith, B. Hess, and E. Lindahl, SoftwareX **1**, 19 (2015).
[19] T. Yamaguchi and Y. Kimura, Mol. Phys. **98**, 1553 (2000).
[20] T. S. Ingebringtsen and H. Tanaka, Proc. Natl. Acad. Sci. U. S. A. **115**, 87–92 (2018).
[21] U. Balucani and M. Zoppi, *Dynamics of the Liquid State* (Oxford University Press, 1994).
[22] T. Yamaguchi, J. Chem. Phys. **145**, 194505 (2016).
[23] D. M. Heyes, J. Chem. Soc. Faraday Trans. II **82**, 1365 (1986).
[24] T. Morita and K. Hiroike, Prog. Theor. Phys. **23**, 1003 (1960).
[25] T. Yamaguchi, J. Chem. Phys. **146**, 094511 (2017).
[26] T. Yamaguchi, M. Saito, K. Yoshida, T. Yamaguchi, Y. Yoda, and M. Seto, J. Phys. Chem. Lett. **9**, 298 (2018).